Physicochem. Probl. Miner. Process., 60(4), 2024, 192381

http://www.journalssystem.com/ppmp

Physicochemical Problems of Mineral Processing

ISSN 1643-1049

Adsorption behaviors of As(III) on bentonite, diatomite, and hematite: implications for scientific remediation of arsenite contamination in soil

Kaibin Fu [1,2], Pengcheng Tang [3], Wei Zhang [1], Shu Chen [1], Gang Tao [1,2], Junfei Liu [4]

[1] Key Laboratory of Solid Waste Treatment and Resource Recycle, Ministry of Education, Southwest University of Science and Technology, Mianyang 621010, China

[2] Tianfu Institute of Research and Innovation, Southwest University of Science and Technology, Chengdu 610299, China

[3] Sichuan Mingxing Electric Power CO., LTD, Suining 629000, China

[4] School of Energy and Environmental Engineering, University of Science and Technology Beijing, Beijing 100083, China

Corresponding author: fukaibin@126.com (Kaibin Fu)

Abstract: Comprehensive understanding of As(III) sorption on natural minerals in contaminated soils is important for scientific decision making in remediation. In this study, the characteristics of As(III) adsorption on three minerals with different crystal structures and chemical compositions (bentonite; diatomite; and hematite) were investigated. The adsorption kinetics and thermodynamics were established. Surface complexation modeling was performed using X-ray diffraction spectroscopy, fourier transform infrared spectroscopy, and X-ray photoelectron spectroscopy. The results showed that the pH value had a more significant effect on As(III) adsorption on hematite than on bentonite and diatomite, and As(III) was efficiently adsorbed by hematite at pH 7.0. The pseudo-first-order model provided an excellent fit to the As(III) adsorption on bentonite and hematite; the diffusion of ions or groups played an important role in the adsorption of As(III) on bentonite and hematite. The adsorption of As(III) on diatomite could be fitted with pseudo-first-order and pseudo-second order kinetic equations, as their regression coefficients were equal (R2=0.999). It was inferred that the adsorption of As(III) on diatomite occurred through solution diffusion and surface chemisorption. The As(III) adsorption on bentonite and diatomite was mainly physical and multilayer adsorption, whereas the As(III) adsorption on hematite was mainly chemical and monolayer absorption. The As(III) adsorption on hematite was divided into two stages: fast and slow. At first, the inner monodentate complex (such as $\equiv$Fe-OAs_3H^-) formed at a high rate, and with the increase in the coverage of As(III) on the surface of iron oxide, the monodentate complex was slowly converted to the bidentate complex. These results verify the possibility of using bentonite, diatomite, and hematite as alternative materials for the remediation of As(III)-contaminated soils, and also indicate that bentonite and diatomite are suitable for the remediation of low As(III)-contaminated soils, while hematite is suitable for the decontamination of high As(III) polluted soil. Selecting suitable remediation materials according to arsenic contamination level is the key to soil scientific remediation.

***Keywords*:** natural minerals, As(III)-adsorbing, kinetics, thermodynamics, scientific remediation

1. Introduction

Long-term exposure to As can cause cancer and malformations of the human nervous system, skin, digestive system, and other internal organs. Hence, As is listed as a priority hazardous contaminant by the World Health Organization (Sharma et al., 2014). In recent years, As concentrations in soil and potable groundwater have increased in many areas around the world, and As pollution has become a global concern (Liu et al., 2021, Loukola-Ruskeeniemi al., 2022). Therefore, there is an urgent need for environmentally friendly materials that would reduce the mobility and bioavailability of As for water or soil treatment. (Wang et al., 2021).

DOI: 10.37190/ppmp/192381

Arsenic can exist in both organic and inorganic forms. In nature, As commonly exists in the form of inorganic compounds. The four oxidation states of inorganic arsenic are As(V) (arsenate), As(III) (arsenite), As(0) (arsenic), and As(-III) (arsine), and the solubility of each form depends on the pH and ionic environment. Among these, As(V) is the most stable form (Zhao et al., 2010). As(Ⅴ) is thermodynamically stable in aerobic water, whereas As(Ⅲ) is predominant in a reductive environment. Inorganic As is more toxic than organic As. As(Ⅲ) is usually more toxic, soluble, and mobile than As(Ⅴ) (Singh et al., 2015). In most of the major reported incidences, As occurs as As(Ⅲ) (Zhang and Jiang, 2022, Singh et al., 2010). Thus, there is an immediate need to develop technologies that are effective for arsenic removal, especially As(III) as well as cater to people's expectation for a better life.

The As-contaminated soil remediation practices are highlighted as two types: in-situ and ex-situ techniques (Liao et al., 2022). The in-situ remediation technology is non-invasive, and involves extracting pollutants in the soil through physical, chemical, biological, or combined methods to reduce the risk of soil pollution (Zhou et al., 2022). Common in-situ extraction applications for As-contaminated soils in recent years included phytoextraction, microbial extraction, and electrokinetic migration. Ex-situ soil remediation technologies refer to excavating the contaminated soil from the original location to other places for subsequent restoration (Amponsah et al., 2018). Common ex-situ soil remediation technologies include ex-situ land farming, ex-situ bio-piles, ex-situ windrow, soil washing, ex-situ composting, ex-situ ion exchange, ex-situ solidification/stabilization, pyrolysis, thermal desorption, et al. (Koul and Taak, 2018).

To date, the solidification/stabilization technique has been widely used for the remediation of As-contaminated soil as a result of its acceptable remediation effect, ease of implementation, cost-effectiveness, and short remediation cycle (Li et al., 2018). Arsenic solidification/stabilization can be achieved by using natural and synthetic amendments such as clay minerals (Xu et al., 2017), Fe/Mn hydroxides (Wang et al., 2019), zeolite minerals (Guo et al., 2019), hydroxylapatite and struvite (Rouff et al., 2016), industrial wastes and by-products (Wu et al., 2017), and biosorbents (Shakoor et al., 2016). Natural minerals have the advantages of low-cost, environmental-friendliness and abundant sourcing. However, there is a lack of up-to-date scientific data on the remediation of As-contaminated soil using natural minerals; moreover, the mechanism for reducing the bioavailability of As remains unclear.

The high groundwater level in some karst areas of Southwest China leads to the formation of soil - water - As(III) coexistence system, and the remediation of As-contaminated soil is quite complicated. As(III) contamination level varies from place to place, and is anisotropic even at the same site. How to select appropriate remediation materials according to arsenite contamination degree and occurrence form has become a research hotspot at home and abroad. The content and forms of arsenic in the soil determine the types and amount of natural minerals used for remediation. Therefore, revealing the interface reaction mechanism between arsenic ions and natural mineral materials is the premise of scientific remediation of arsenic contaminated soil. In general, arsenic sorption mechanisms onto soil minerals are of paramount importance because these processes regulate As soil mobility, which further affects the bioavailability and potential toxicity of As (Rahman et al., 2017a, 2017b). An As(III) to As(V) oxidation stage is deemed necessary to achieve satisfactory remediation results (Xiao et al., 2022). However, numerous studies have indicated that As(III) oxidation might not be the only way for decontaminating soils, both oxidation or As(III) direct sorption could be the options (Li et al., 2023).

Modeling the adsorption characteristics of As(III) from aqueous solution on natural minerals is important to reveal the mechanism of arsenic remediation in contaminated soils, and to guide scientific remediation projects in high groundwater level karst areas of Southwest China. Consequently, three minerals with different crystal structures and chemical compositions: bentonite, diatomite, and hematite, were selected as amendments for the remediation of As(Ⅲ)-contaminated soil. The objective of this study was to identify As(III) adsorption behavior (kinetics, thermodynamics, and mechanisms) in three natural surfaces based on different approaches, and to guide the scientific remediation of As(III)-contaminated soil.

2. Materials and methods

2.1. Materials

Bentonite was obtained from Tiandong, Guangxi (China). Diatomite was obtained from Miyi. (Sichuan, China). Hematite was purchased from Hubei Jusheng Technology Co. LTD (China). The three natural

minerals, used without modification, were milled to pass through a 200-mesh nylon sieve. The main chemical constituents of these three minerals are shown in Table1.

Table 1. The main composition of three minerals (%)

Compounds	SiO_2	Al_2O_3	Fe_2O_3	CaO	MgO	K_2O	Na_2O	MnO
Bentonite	59.64	20.30	8.60	3.83	1.54	3.97	0.83	0.46
Diatomite	77.86	12.51	2.89	0.75	0.89	2.69	0.64	0.12
Hematite	35.88	7.30	38.19	6.46	1.14	1.79	4.19	0.34

Analytical grade chemicals were used in the experiments unless stated otherwise. H_2SO_4 (98% v/v), NaOH, and KBr were purchased from China National Pharmaceutical Group Co. Ltd. (Sinopharm). The As(III) standard solution (1000 μg/mL) was purchased from Guobiao (Beijing) Testing & Certification Co., Ltd. Deionized water was used throughout the experiment.

2.2. Sorption experiments

2.2.1. Sorption edges

On the basis of the previous studies, the effect of pH on adsorption of As(III) on bentonite, diatomite, and hematite was studied at the initial As(III) concentration of 10 mg/L, temperature of 25 °C, and rotation speed of 165 rpm. The adsorbent concentration was 2 g/L. The pH of the adsorption solution (100 mL) was adjusted using HCl and KOH. Following the adsorption experiments, the suspensions were centrifuged at 4000 rpm for 10 min and passed through a 0.45 μm filter. The filtrates were collected for analysis of aqueous As(T), As(III), and As(V).

2.2.2. Sorption kinetics

The adsorption amount (q) and adsorption rate (η) of As(III) were calculated using Eqs. 1 and 2. To ensure the accuracy, repeatability, and reproducibility of the adsorption data, all adsorption experiments were conducted in triplicate. The limit of the experimental error in triplicate was ±5%.

$$q = \frac{(C_0 - C_e)\cdot V}{m} \tag{1}$$

$$\eta = \frac{C_0 - C_e}{C_0} \times 100\% \tag{2}$$

where C_0 (mg/L) and C_e (mg/L) are the initial and equilibrium concentrations, respectively; V (L) is the volume of the solution; m(g) is the mass of the adsorbent; and η (%) is the removal rate.

The kinetics of As(III)-adsorption was studied in a solution containing As(III) at pH 7.0 and 25°C, the adsorption amount of As(III) was calculated using Eq. 1. Subsequently, the pseudo-first-order (PFO, Eq. 3) and pseudo-second-order (PSO, Eq. 4) kinetic model were used to describe the adsorption behavior.

$$q_t = q_e[1 - \exp(-k_1 t)] \tag{3}$$

$$q_t = k_2 {q_e}^2 t/[1 + k_2 q_e t)] \tag{4}$$

where q_t (mg/g) is the adsorption capacity, t (h) is the adsorption time, q_e (mg/g) is the theoretical adsorption capacity, K_1 and K_2 are the adsorption rate constants of PFO and PSO kinetics, respectively.

2.2.3. Sorption isotherms

The isotherms were studied at pH 7.0 for 6.0 h under initial As(III) concentration of 5, 10, 20, 50, 100, and 150 mg/L. The test temperatures were 25, 30, and 35°C. After the adsorption experiments, the As(III)-adsorption amounts at different initial concentrations and temperatures were calculated. The Langmuir (Eq. 5), and Freundlich models (Eq. 6) were used to fit the adsorption data.

$$\frac{C_e}{q_e} = \frac{C_e}{Q_{max}} + \frac{1}{Q_{max} K_l} \tag{3}$$

$$\log(q_e) = \log(K_f) + \frac{1}{n}\log(C_e) \tag{4}$$

where Q_e (mg/g) is the equilibrium adsorption capacity, C_e (mg/L) is the equilibrium concentration, Qmax (mg/g) is the saturated adsorption capacity, K_l (L/mg) is the adsorption equilibrium constant, n is the characteristic adsorption coefficient, and K_f is the adsorption coefficient.

2.3. Analytical methods and quality assurance

The As(T) was analyzed using inductively coupled plasma emission spectrometer (ICP-AES, iCPA6500 Thermo Fisher, USA). The quantification of aqueous arsenic species (As(III) and As(V)) was analyzed by hydride generation-atomic fluorescence spectrometry coupled with high-performance liquid chromatography (HPLC-AFS, Jitian, China). The corresponding standard curves were prepared by the As(T), As(III), and As(V) standard solution (GBW08611, BW5325-1, and BW5341-1) purchased from National Institute of Metrology, China, and the determination coefficient of the curve equation was 0.999. The relative standard deviation of these measurements was always better than 5%.

The mineral composition and crystal structure were analyzed using a XRD (X´Pert PRO, PANalytical B.V., Netherlands). The molecular environment of a single mineral surface before and after As(III) adsorption was analyzed using FTIR (Spectrum One, PerkinElmer, Inc., USA). XPS (ultra-DLD, Shimadzu, Japan) was used to determine the surface binding energies.

3. Results and discussion

3.1. Effect of pH

The tentative adsorption time was 2 hours. The effect of pH on As(III) removal rate is shown in Fig. 1. As shown in Fig. 1, the efficiencies of As(III) adsorption on bentonite and diatomite were poor, at only 17 and 12%, respectivly. Among the three adsorbents, hematite showed the best As(Ⅲ) adsorption efficiency, reaching 68% at pH 7.0. The pH value is the main factor affecting the adsorption of As(III) on hematite (Liu et al., 2020). This effect is attributed to the form of As(III) in the aqueous solution. As(III) mainly exists in the form of H3AsO3 under acidic or neutral conditions. Under alkaline conditions (pH > 7), $As(OH)_3$ partially ionizes to $H_2AsO_3^-$. At pH of 9, the content of $H_2AsO_3^-$ reachs 50%, and only small amounts of $H_2AsO_3^-$ are present in the strongly alkaline conditions (pH > 11.0) (Mirazimi and Liu, 2021).

With an increase in pH, the adsorption efficiency of A(III) on the hematite surface first increased and then decreased, reaching the maximum at pH 7.0. In a strongly acidic environment (pH < 3.0), hematite may dissolve and lose some adsorption sites, resulting in a relatively low adsorption efficiency. In weakly acidic environments with a pH of 2.0–7.0, the surface of hematite has a more positive charge; and the electrostatic interaction and polarization effect lead to an increase in the adsorption efficiency of H3AsO3 on hematite. Under alkaline conditions (pH > 7.0), the hematite surface is negatively charged, leading to a reduction in the adsorption efficiency of A(III) (Han et al., 2022). The negative charge of the mineral surface results in a low adsorption efficiency of As(III) on bentonite and diatomite (Memedi et al., 2022).

The results of the analysis of As valence state in the supernatant after adsorption are shown in Fig. 2. Figures 2(a) and 2(b) demonstrate that only a very small amount of As(V) was generated during the

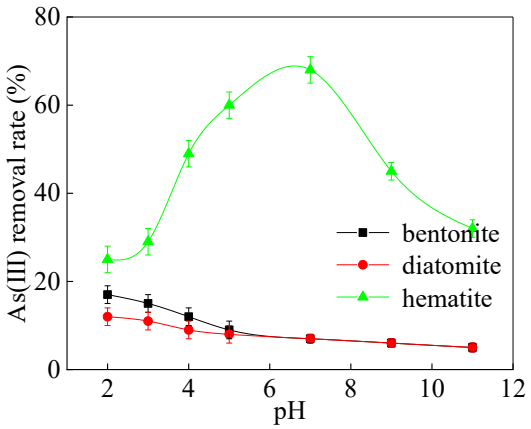

Fig. 1. Effect of pH on As(III) adsorption efficiency

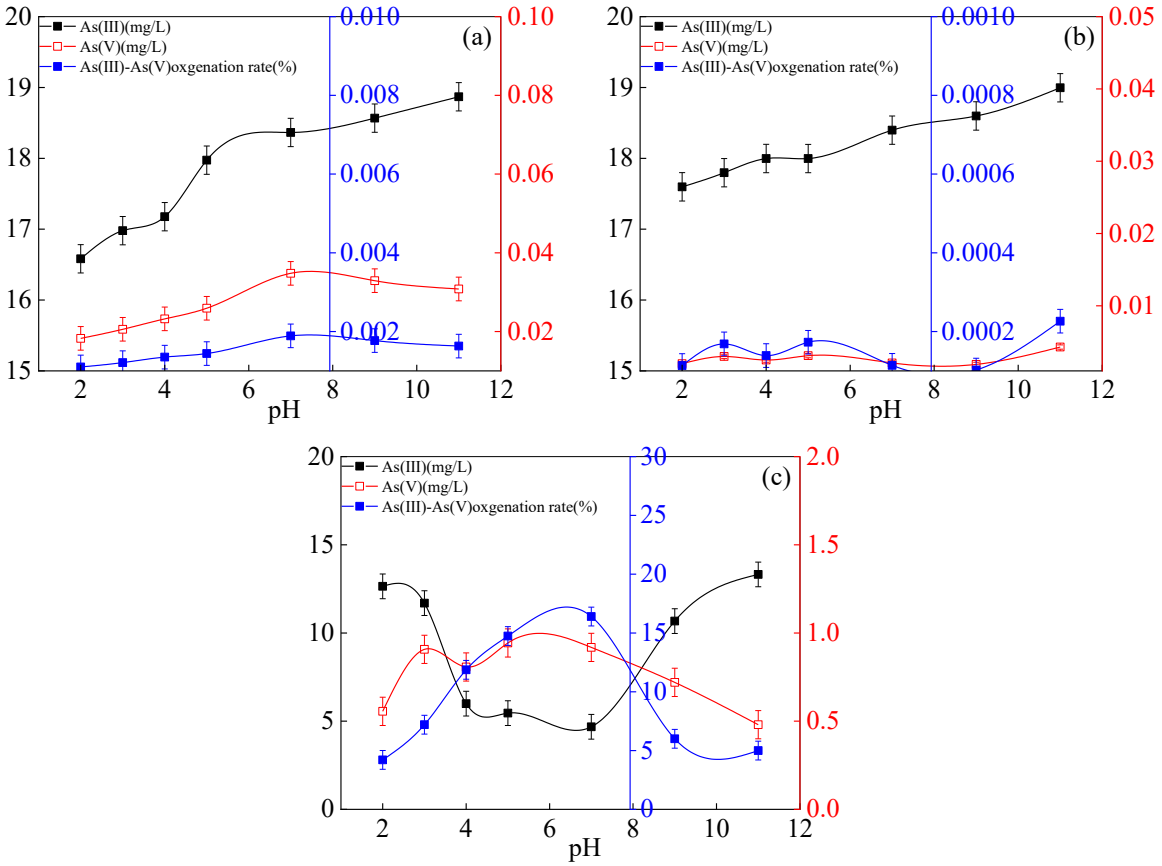

Fig. 2. Effect of pH on As(III) oxgenation rate (a-bentonite, b-diatomite, c-hematite)

adsorption of As(III) on bentonite and diatomite. The surface of diatomite was covered with silica hydroxyl, which is a weak oxidant. Montmorillonite, an important component of bentonite, plays a major role in adsorption. The ability of montmorillonite to oxidize As(III) to As(V) is very weak. As shown in Fig. 2(c), As(III) was detected under different pH conditions in the hematite–As(Ⅲ) interaction system, which means that hematite could oxidize part of As(III) to As(Ⅴ). The oxidation rate of A(III) first increased, and then decreased with the increase in pH value. At pH 7.0, the oxidation rate of As(III) reached 16.4%. These results showed that As(III) oxidation might not be efficient and enough for soil decontamination, so As(III) sorption should also be considered when choosing the natural minerals.

3.2. As(III) sorption kinetics and solid-phase association on minerals

As(III) sorption kinetics on bentonite, diatomite, and hematite at pH = 7.0 are shown in Fig. 3. As shown in Fig. 3, the quantity of As(III) adsorbed rapidly increases early on for bentonite and hematite, followed by a gradual or somewhat slower reaction. The adsorption kinetics of As(III) on bentonite and hematite were similar, whereas, the adsorption kinetics of As(III) on diatomite significantly differed, and the adsorption capacity of As(III) reached saturation after approximately 12–18 min.

The kinetic model parameters and regression coefficients (R2) for As(III) adsorption on bentonite, diatomite, and hematite at pH=7.0 (Table 2) were derived from the linear fitting curves for the PFO and PSO kinetics. The regression coefficients (R^2) showed that PSO does not accurately describe the kinetics

Table 2. Parameters and regression coefficients (R^2) of kinetic models for As(III) adsorption at pH 7.0

element	Minerals	$q_t=q_e[1-\exp(-k_1t)]$			$q_t=k_2q_e^2t/(1+k_2q_et)]$		
		k_1(/h)	Q_{cal}(mg/g))	R^2	k_2/(g·(mg/h))	Q_{cal}(m/·g)	R^2
As(III)	bentonite	0.90	1.37	0.972	0.464	1.75	0.951
	diatomite	21.17	0.63	0.999	281.59	0.63	0.999
	hematite	0.93	3.75	0.997	0.208	4.50	0.986

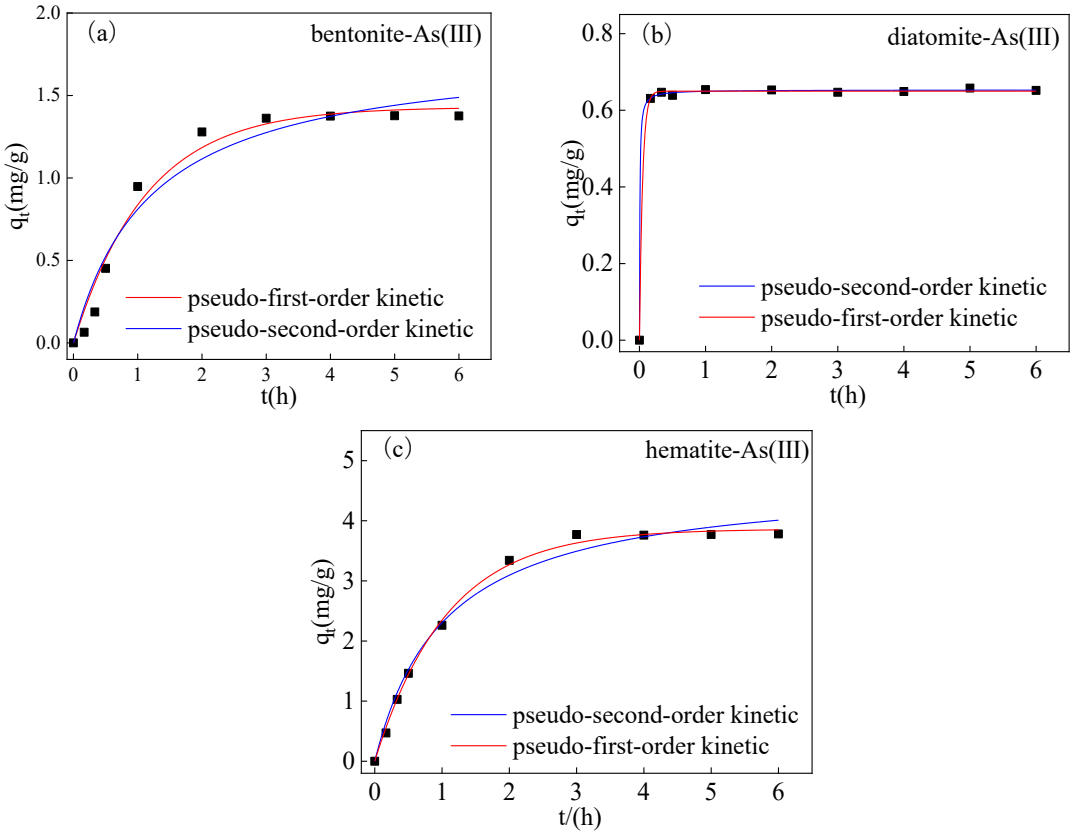

Fig. 3. Fitting curves of PFO and PSO adsorption kinetics (pH = 7.0)

of As(III) adsorption on bentonite and hematite, as evidenced by the poor model fit (Table 2); at the same time, the PFO model provided excellent fits for As(III) adsorption on bentonite and hematite. These results indicate that the diffusion of ions or groups plays an important role in the adsorption of As(III) on bentonite and hematite. The adsorption of As(III) on diatomite was well-fitted with both PFO and PSO kinetic equations, and their regression coefficients (R^2) were the same (R^2 = 0.999). This suggests that the adsorption of As(III) on diatomite occurred through solution diffusion and surface chemisorption.

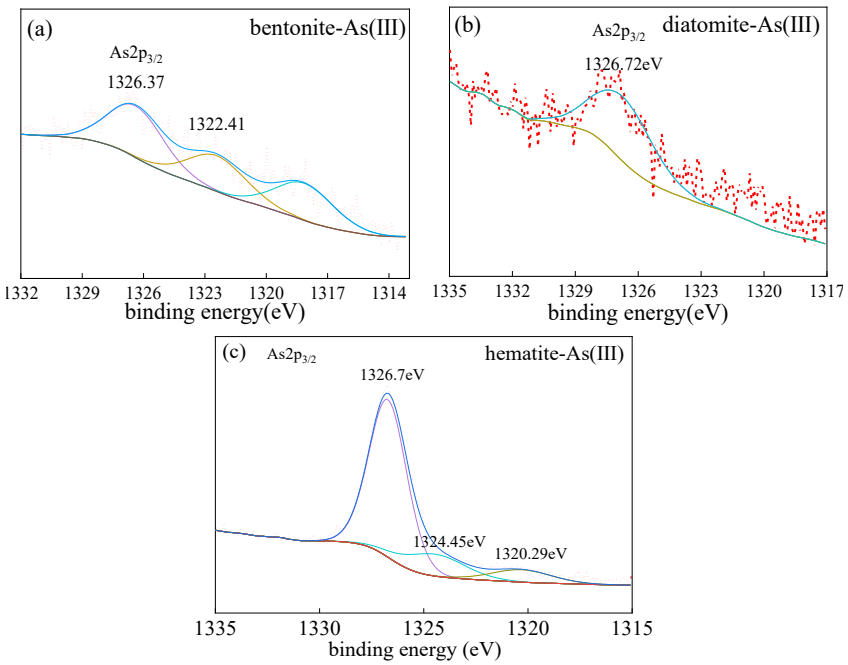

Fig. 4. As2$p_{3/2}$ spectra of (a) bentonite, (b) diatomite, and (c) hematite after As(III) adsorption

As2p$_{3/2}$ spectra of bentonite, diatomite, and hematite(c) after As(III) adsorption are shown in Fig. 4. The As2p$_{3/2}$ binding energies of bentonite, diatomite, and hematite after As(III) adsorption were 1326.37, 1326.72, and 1326.70eV, respectively. This might indicate that As(Ⅲ) is present on the surfaces of bentonite, diatomite and hematite (Wagner et al., 1979). No characteristic peak of As(V) was detected. This result confirms that bentonite and diatomite did not oxidize As(III) to As(V), and that As(V) produced through the oxidation of As(Ⅲ) by hematite might below the XPS detection limit.

3.3. The As(III) adsorption thermodynamics

The Langmuir and Freundlich models of As(III) on the surface of bentonite, diatomite, and hematite are shown in Fig. 5, and their adsorption thermodynamic parameters are listed in Table 3.

The correlation coefficients (R^2) of the Freundlich model for the adsorption of As(III) on bentonite and diatomite were higher than those of the Langmuir model. This held in the temperature range of 25–35°C. Thus, the Freundlich model was consistent with the experimental data and could describe the As(III) adsorption on bentonite and diatomite. These results show that the adsorption of As(III) on bentonite and diatomite was mainly physical and multilayer adsorption.

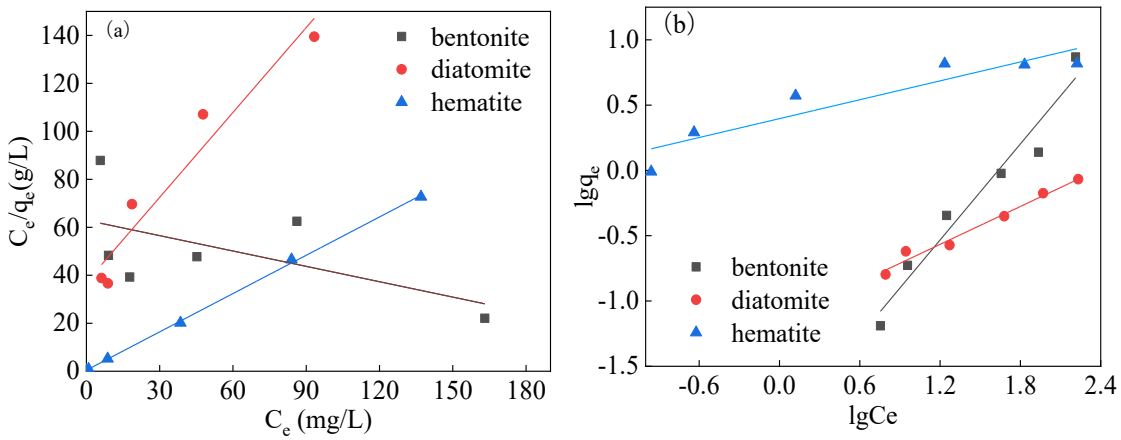

Fig. 5. (a) Langmuir model and (b) Freundlich model of As(III) adsorption on bentonite, diatomite and hematite at pH 7.0 and 25°C for 6.0 h

Table 3 Isotherms of (a) Langmuir model and (b) Freundlich model of As(III) adsorption on bentonite, diatomite, and hematite

element	minerals	Temperature (°C)	Langmuir model			Freundlich model		
			Q_{max}(mg/g)	K_L(L/mg)	R^2	n	K_f	R^2
As(Ⅲ)	bentonite	25	-	-	0.179	0.82	0.01	0.942
		30	-	-	-	0.87	0.04	0.964
		35	-	-	-	0.91	0.06	0.972
	diatomite	25	0.85	0.032	0.915	2.06	0.07	0.973
		30	0.85	0.041	0.964	2.11	0.08	0.981
		35	0.87	0.037	0.962	2.15	0.08	0.967
	hematite	25	6.59	1.43	0.999	4.15	2.49	0.823
		30	5.77	1.54	0.986	4.31	2.47	0.855
		35	6.61	1.57	0.998	4.43	2.51	0.841

Note: - indicates that the correlation is too poor to fit

At the temperatures of 25, 30, and 35°C, the correlation coefficients (R2) of the Langmuir model for As(III) adsorption on hematite were 0.999, 0.986, and 0.998, respectively, whereas those of the Freundlich model were 0.823, 0.855, and 0.841, respectively (Table 3). Thus, the correlation coefficients (R2) of the Langmuir model for As(III) adsorption on hematite were higher than those of the Freundlich model. The Langmuir model was therefore in better agreement with the experimental data and could describe the As(III) adsorption on hematite. The adsorption of As(III) on hematite was mainly chemical and monolayer absorption.

3.4. XRD and FTIR analysis

Information on As(III) and As-containing species is essential for elucidating the reaction mechanisms. XRD and FTIR were used to further confirm the formation of As-containing compounds on the surface of bentonite, diatomite, and hematite after As(III) adsorption.

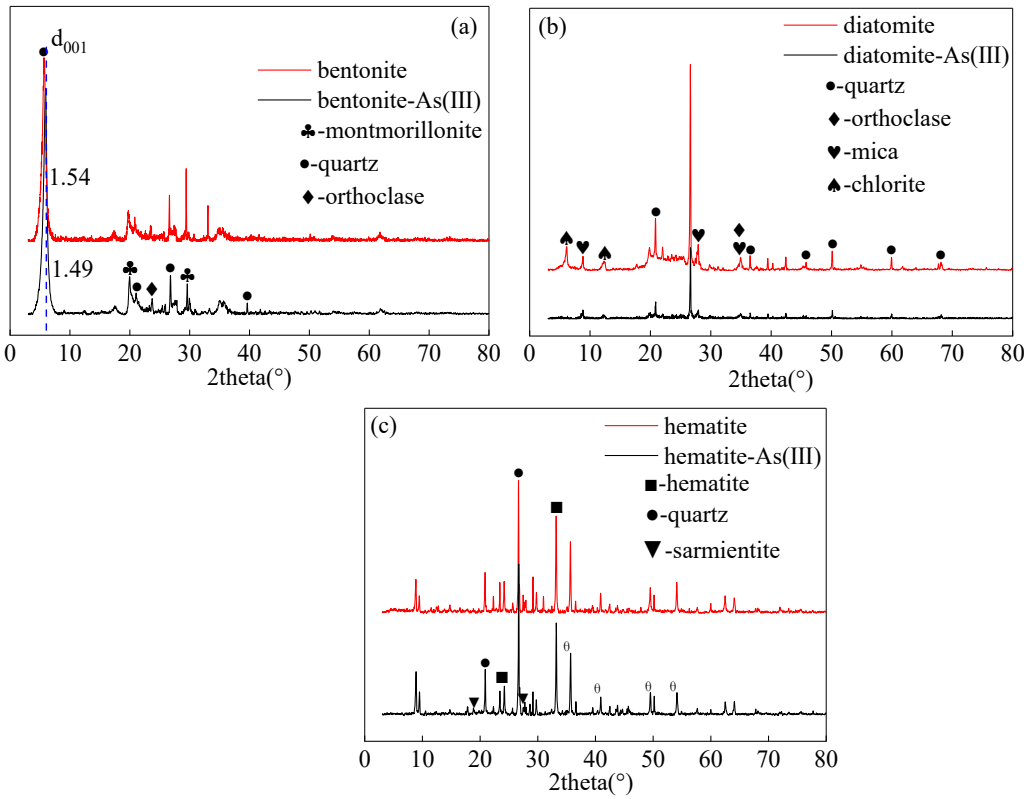

Fig. 6. XRD spectra of (a) bentonite, (b) diatomite, and (c) hematite before and after As(III) adsorption

The XRD spectrum of bentonite before As(III) adsorption in Fig. 6(a) shows the diffraction peaks of montmorillonite at the 2θ angle of 5.94, 19.95, 29.56° and those of quartz at 21.10 and 26.83° were observed. After As(III) adsorption, the distance d001 between layers expanded from 14.9 Å (1.49 nm) to 15.4 Å (1.54 nm). As(III) mainly exists as arsenite molecules in aqueous solutions with pH < 9 and in the form of arsenite anions at higher pH values (pH ≥ 9). In general, neither can exchange ions with the montmorillonite layer cation, possibly because arsenite molecules or ions enter montmorillonite layers through physical adsorption, leading to a change in the layer spacing. Figure 6(b) shows that diatomite mainly consisted of quartz mixed with a small amount of orthoclase, mica, chlorite, and other minerals. Comparing the XRD patterns of diatomite before and after As(III) adsorption, the corresponding peak positions of diatomite did not change significantly. However, the characteristic peak of the amorphous SiO_2 in diatomite, the "steamed bun", in the range of 19.16–29.20°, was very distinct. The "steamed bun" of the amorphous SiO2 disappeared in the XRD pattern of diatomite after As(III) adsorption, perhaps due to the interaction of amorphous silica surface hydroxyl groups with As(III). These results indicated that As(III) adsorption on diatomite led to changes in its composition and structure. Figure 6(c) shows that the characteristic diffraction peaks of hematite (Fe_2O_3) appear at 24.13, 33.19, 35.70, and 40.91°, while the characteristic diffraction peaks of quartz appear at 20.92 and 26.70°. After As(III) adsorption, new peaks were observed, the diffraction peaks of sarmientite ($Fe_2[AsO_4][SO_4]OH \cdot 5H_2O$) appear at 19.112, 27.506, 27.681°. No diffraction peaks of As(III) were observed due to low concentration.

Previous studies have suggested that As(III) has stronger adsorption on the surface of hematite (Goldberg and Johnston, 2001). Therefore, FTIR analysis was used to further illustrate the selective adsorption of As(III) on a single mineral. Figure 7(a) shows that the absorption peaks appearing at 3633 cm^{-1} correspond to the antisymmetric stretching vibration absorption peaks of the –OH of the interlayer water molecules. The absorption peaks at 914 cm^{-1} correspond to the stretching vibration absorption peaks of –OH in the Al–O–H of bentonite. The Si–O–Si stretching vibration peak with a wave

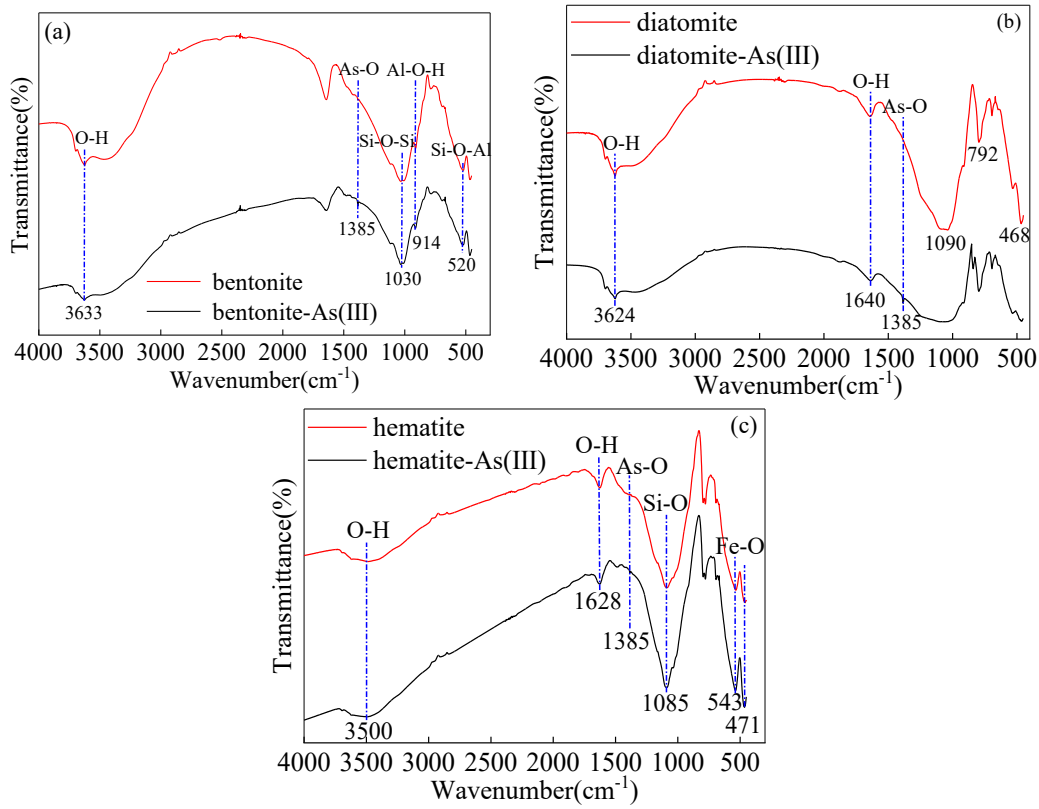

Fig. 7. FTIR spectra of (a) bentonite, (b) diatomite, and (c) hematite before and after As(III) adsorption

that the absorption peak at 3624 cm^{-1} corresponds to the antisymmetric stretching vibration of –OH number of 1030 cm^{-1} and the Si–O–Al bending vibration with a wave number of 520 cm^{-1} are the characteristic peaks of bentonite (Zhu et al., 2017). After the adsorption of As(III), a new absorption peak appeared at 1385 cm^{-1}, which was mainly attributed to the stretching vibration of the As–O bond, indicating that a new chemical bond, As–O, was formed on the surface of bentonite. Figure 7(b) showson the surface of diatomite. The absorption peak at 1640 cm^{-1} was attributed to the antisymmetric stretching vibration of −OH in water molecules. Peaks at 1090, 792, and 468 cm^{-1} are the vibration absorption peaks of the Si–O bond. The FTIR spectra of hematite before and after As(III) adsorption are shown in Fig. 7(c). The absorption peaks at 471 and 543 cm^{-1} were attributed to Fe–O vibrations and are characteristic bands of hematite (Rufus et al., 2017). After the adsorption of As(III), the new absorption peak at 1385 cm−1 appeared on the surface of diatomite and hematite, the same as that in bentonite, which is the stretching vibration of the As–O bond, indicating that As(III) might be adsorbed on the surface of diatomite and hematite by surface complexation.

4. Implications for scientific remediation of As(III) contamination

Bentonite is mainly composed of montmorillonite, which has a 2:1 crystal structure: two layers of silica tetrahedrons and one layer of aluminum oxide octahedra in between. Owing to the layered structure, montmorillonite may contain cations, such as Mg^{2+}, Na^{+}, and K^{+}, and its crystal surface is covered with –SiOH. The main component of diatomite is porous amorphous silica, and its surface is covered with a large number of silicon hydroxyl groups (Gao, 2006). Hydrolysis of the silicon hydroxyl group produces linked and twin siloxy groups that lead to the generation of surface charge in diatomite particles and formation of abundant adsorption sites. Therefore, bentonite and diatomite mainly interact with heavy metal ions through physical adsorption, ion exchange, and surface complexation. A previous study indicated that As(III) adsorption on bentonite and diatomite is closely related to its speciation in aqueous solutions. As(III) is stable at pH < 9 in the form of neutral H_3AsO_3, at pH = 9–12 as H_2AsO^{3-}, at pH = 12–13 as $HAsO_3^{2-}$, and at pH > 13 as AsO_3^{3-} (Asere et al., 2019). The pH value is less than the point of zero charge (PZC), H_3AsO_3 enters bentonite layers through the electrostatic interaction and polarization effect, resulting in an increase in the distance between bentonite layers (Gao, 2006). With

an increase in pH, pH > PZC, the surface of bentonite and diatomite have more negative charge, electrostatic repulsion reduces the adsorption efficiency. At this time, the adsorption between the two minerals and As(III) maybe mainly weak hydrogen bonding. These results indicate that bentonite and diatomite are suitable for soil remediation with low As(III) contamination.

Heavy metal ion adsorption on hematite is mainly divided into inner-sphere obligate adsorption and outer-sphere nonobligate adsorption (Goldberg and Johnston, 2001, Mo, et al., 2021). The inner-sphere obligate adsorption refers to the adsorption of heavy metal ions into the mineral double electric layer through the exchange of ligands with hematite surface functional groups (e.g., ≡Fe-OH) or the formation of chemical bonds (Liu, et al., 2023), which is chemical adsorption. Outer sphere non-obligate adsorption refers to the adsorption of heavy metal ions at a certain distance from the surface of iron oxide minerals through electrostatic attraction, which is physical adsorption (Yang, et al., 2017). For non-obligate adsorption, the zero-potential pHpzc is the key factor affecting the adsorption behavior of heavy metal ions on the mineral surface. The pHpzc of hematite is typically between 6 and 8, and the pHpzc of hematite used in the experiment was approximately 7.0 (Dixit and Hering, 2003). The pH value of the adsorption test solution was below pHpzc, and As(III) adsorption on hematite might be obligate adsorption. The adsorption kinetics and thermodynamics further verified that As(III) adsorption on hematite was mainly chemical adsorption (obligate adsorption) supplemented by non-obligate adsorption (Fang, et al., 2022). As(III) adsorption on hematite occurred in two stages: fast and slow. At first, the inner monodentate complex (such as ≡Fe-OAs$_3$H$^-$) was formed at a high rate, and with the increase in the coverage of As(III) on the surface of iron oxide, the monodentate complex was slowly converted to the bidentate complex (Fig. 8). These results indicate that hematite can be used to remediate soil with high As(III) contamination.

$$\equiv\text{Fe-OH} + \text{AsO(OH)}_2^- \leftrightarrow \equiv\text{Fe-O-AsO(OH)}^- + \text{H}_2\text{O} \quad (7)$$

$$\equiv\text{Fe-OH} + \text{As(OH)}_3 \leftrightarrow \equiv\text{Fe-O-As(OH)}_2 + \text{H}_2\text{O} \quad (8)$$

$$\equiv\text{Fe-OH} + \text{AsO}_2\text{(OH)}_2^- \leftrightarrow \equiv\text{Fe-O-AsO}_2^{2-} + \text{H}_2\text{O} \quad (9)$$

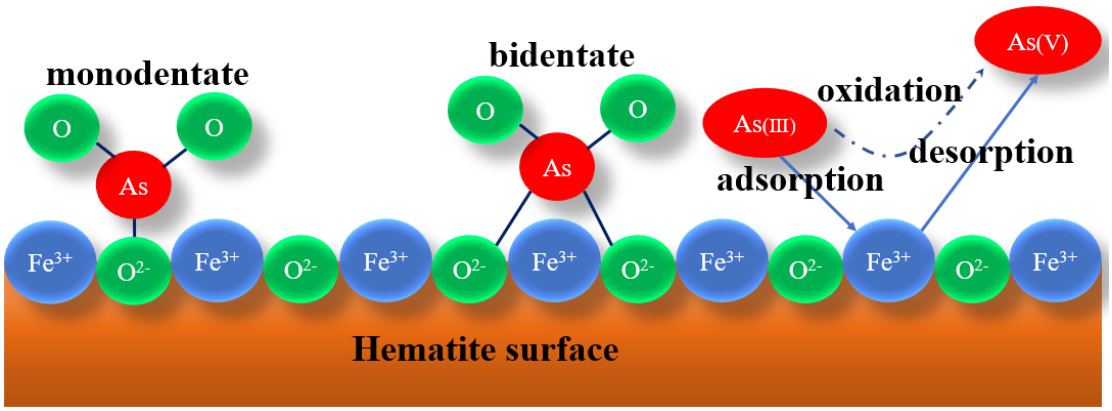

Fig. 8. Schematic of the adsorption of As on hematite

5. Conclusions

The pH value was found to significantly affect the As(III) adsorption behavior on the three minerals and have a more significant effect on the As(III) adsorption on hematite than on bentonite and diatomite. As(III) was efficiently adsorbed by hematite at pH = 7.0. The results of the adsorption kinetics analysis showed that the PFO model provided excellent fits for As(III) sorption on bentonite and hematite, and that the diffusion of ions and groups plays an important role in the adsorption of As(Ⅲ) on bentonite and hematite. The adsorption of As(III) on diatomite was well fitted using both PFO and PSO kinetic equations, with equal regression coefficients (R^2 = 0.999). It was inferred that the adsorption of As(III) on diatomite occurred through solution diffusion and surface chemisorption.

The adsorption thermodynamics showed that the As(III) adsorption on bentonite and diatomite was mainly physical and multilayer adsorption, whereas the As(III) adsorption on hematite was mainly chemical and monolayer absorption. The As(III) adsorption on hematite was divided into two stages: fast and slow. At first, the inner monodentate complex (such as ≡Fe-OAs$_3$H$^-$) formed at a high rate,

and with the increase in the coverage of As(III) on the surface of iron oxide, the monodentate complex was slowly converted to the bidentate complex.

These results verified the possibility of using bentonite, diatomite, and hematite as alternative materials for the remediation of As(III)-contaminated soils. Based on the adsorption behavior of As(III) on three mineral surfaces, bentonite and diatomite are suitable for the remediation of low As(III)-contaminated soils, while hematite is suitable for the decontamination of high As(III) polluted soil.

Acknowledgements

This research was supported by the Ganzi Prefecture Science and Technology Project (210031, and 220012), and the Sichuan Science and Technology Program (No. 2023YFG0357), and, the National Key R&D Program of china (No. 2023YFC3207300).

References

AMPONSAH, N.Y., WANG, J.Y., ZHAO, L., 2018. *A review of life cycle greenhouse gas (GHG) emissions of commonly used ex-situ soil treatment technologies*. J. Clean. Prod. 186, 514-525.

ASERE, T.G., STEVENS, C.V., LAING, G.D., 2019. *Use of (modified) natural adsorbents for arsenic remediation: A review*. Sci. Total Environ. 676, 706-720.

DIXIT, S., HERING, J.G., 2003. *Comparison of As(V) and As(III) sorption onto iron oxide minerals: implications for arsenic mobility*. Environ. Sci. Technol., 37: 4182-4189.

FANG, L.P., GAO, B.L., LI, F.B., LIU, K., CHI, J.L., 2022. *The nature of metal atoms incorporated in hematite determines oxygen activation by surface-bound Fe(II) for As(III) oxidation*. Water Res., 227, 119351.

GAO, W., 2006. *Study on adsorption of diatomite and bentonite for uranium*. University of South China, Hengyang Hunan, China.

GOLDBERG, S., JOHNSTON, C.T., 2001. *Mechanisms of arsenic adsorption on amorphous oxides evaluated using macroscopic measurements, vibrational spectroscopy, and surface complexation modeling*. J. Colloid Interf. Sci. 234, 204 - 216.

GUO, X.F., CUI, X.Y., LI, H.S., XIONG, B.H., 2021. *Purifying effect of biochar-zeolite constructed wetlands on arsenic-containing biogas slurry in large-scale pig farms*. J. Clean. Prod. 279, 123579.

HAN, D.S., ABDEL-WAHAB, A., BATCHELOR, B., 2010. *Surface complexation modeling of arsenic(III) and arsenic(V) adsorption onto nanoporous titania adsorbents (NTAs)*. J. Colloid Interf. Sci. 348, 591–599.

HAN, W.J., ZHU, Y.M., LIU, J., LI, Y.J., 2022. *A novel depressant HPAM of the hematite in reverse cationic flotation of iron ore*. Colloid. Surface. A 641, 128547.

KOUL, B., TAAK, P., 2018. *Biotechnological Strategies for Effective Remediation of Polluted Soils*. Springer.

LI, J.S., WANG, L., CUI, J.L., POON, C.S., BEIYUAN, J., TSANG, D.C.W., LI, X.D., 2018. *Effects of low-alkalinity binders on stabilization/solidification of geogenic As-containing soils: spectroscopic investigation and leaching tests*. Sci. Total Environ. 631–632, 1486–1494.

LI, X.L., WANG, C.Q., CHEN, X.L., LI, D.Y., JIN Q., 2023. *Enhanced oxidation and removal of As(Ⅲ) from water using biomass-derived porous carbon-supported nZVI with high iron utilization and fast adsorption*. J. Environ. Chem. Eng., 11, 109038.

LIAO, X., LI, Y.M., MIRANDA - AVILES, R., ZHA, X.X., ANGUIANO, J.H.H., SANCHEZ, C.D.M., PUY - ALQUIZA, M.J., GONZALEZ, V.P., LUISA FERNANDA RUEDA GARZON, L.F.R., 2022. *In situ remediation and ex situ treatment practices of arsenic-contaminated soil: An overview on recent advances*. J. Hazard. Mater. Adv. 8, 100157.

LIU, G., MENG, J., HUANG, Y., DAI, Z., TANG, C., XU, J., 2020. *Effects of carbide slag, lodestone and biochar on the immobilization, plant uptake and translocation of As and Cd in a contaminated paddy soil*. Environ. Pollut. 266, 115194.

LIU, L., YANG, Z. H., ZHAO, F. P., CHAI, Z. T., YANG, W. C., XIANG, H. R., LIAO, Q., SI, M. Y., LIN, Z. 2023. *Manganese doping of hematite enhancing oxidation and bidentate-binuclear complexation during As(III) remediation: Experiments and DFT calculation*. Chem. Eng. J. 471, 144758.

LIU, Y.C., TIAN, X., CAO, S.W., LI, Y., DONG, H.j., LI, Y.S., 2021. *Pollution characteristics and health risk assessment of arsenic transformed from feed additive organoarsenicals around chicken farms on the North China Plain*. Chemosphere, 278, 130438.

LOUKOLA - RUSKEENIEMI, K., MULLER, I., REICHEL, S., JONES, C., BATTAGLIA - BRUNET, F., ELERT, M., GUEDARD, M.L., HATAKKA, T., HELLAL, J., JORDAN, I., KAIJA, J., KEISKI, R.L., PINKA, J., TARVAINEN, T., TURKKI. A., TURPEINEN, E., VALKAMA, H., 2022. *Risk management for arsenic in agricultural soil–water systems: lessons learned from case studies in Europe*. J. Hazard. Mater. 424(D), 127677.

MEMEDI, H., REKA, A.A., KUVENDZIEV, S., ATKOVSKA, K., GARAI, M., MARINKOVSKI, M., PAVLOVSKI, B., LISICHKOV, K., 2022. *Chapter 3 - Adsorption of Cr(VI) ions from aqueous solutions by diatomite and clayey diatomite. Biological Approaches to Controlling Pollutants: Advances in Pollution Research*, 29-48.

MIRAZIMI, M., LIU, W.Y., 2021. *Aqueous arsenic and sulfur speciation analysis and solid phase characterization in the dissolution of arsenic trisulfide*. Hydrometallurgy 199, 105545.

MO, X.X., SIEBECKER, M.G., GOU, W.X., LI, L., LI, W. 2021. *A review of cadmium sorption mechanisms on soil mineral surfaces revealed from synchrotron-based X-ray absorption fine structure spectroscopy: Implications for soil remediation*. Pedosphere, 31, 11-27.

RAHMAN, M.S., CLARK, M.W., YEE, L.H., COMARMOND, M.J., PAYNE, T.E., KAPPEN, P., MOKHBER - SHAHIN, L., 2017a. *Arsenic solid-phase speciation and reversible binding in long-term contaminated soils*. Chemosphere 168, 1324-1336.

RAHMAN, M.S., REICHELT - BRUSHET, A.J., CLARK, M.W., FARZANA, T., YEE, L.H., 2017b. *Arsenic bio-accessibility and bioaccumulation in aged pesticide contaminated soils: a multiline investigation to understand environmental risk*. Sci. Total Environ. 581, 782-793.

ROUFF, A.A., MA, N., KUSTKA, A.B., 2016. *Adsorption of arsenic with struvite and hydroxylapatite in phosphate bearing solutions*. Chemosphere 146, 574-581.

RUFUS, A., SREEJU, N., VILAS, V., PHILP, D., 2017. *Biosynthesis of hematite (a-Fe_2O_3) nanostructures: size effects on applications in thermal conductivity, catalysis, and antibacterial activity*. J. Mol. Liq. 242, 537-549.

SHAKOOR, M.B., NIAZI, N.K., BIBI, I., MURTAZA, G., KUNHIKRISHNAN, A., SESHADRI, B., SHAHID, M., ALI, S., BOLAN, N.S., OK, Y.S., ABID, M., ALI, F., 2016. *Remediation of arsenic contaminated water using agricultural wastes as biosorbents*. Crit. Rev. Environ. Sci. Technol. 46, 467-499.

SHARMAa, A.K., TJELL, J.C., SLOTH, J.J., HOLM, P.E., 2014. *Review of arsenic contamination, exposure through water and food and low cost mitigation options for rural areas*. Appl. Geochem. 41, 11-33.

SINGH, R., SINGH, S., PARIHAR, P., SINGH, V.P., PRASAD, S.M., 2015. *Arsenic contamination, consequences and remediation techniques: A review*. Ecotox. Environ. Safe. 112, 247-270.

WAGNER, C.D., RIGGS, W.M., DAVIS, L.E., MOULDER, J.F., MUILENBERG, G.E., 1979. *Handbook of X-ray Photoelectron Spectroscopy*. Perkin-Elmer Corporation Physical Electronics Division, U.S.A.

WANG, L., CHO, D.W., TSANG, D.C., CAO, X., HOU, D., SHEN, Z., ALESSI, D.S., OK, Y.S., POON, C.S., 2019a. *Green remediation of As and Pb contaminated soil using cement-free clay-based stabilization/solidification*. Environ. Int. 126, 336-345.

WANG, X., YU, H., LI, F., LIU, T., WU, W., LIU, C., LIU, C., ZHANG, X., 2019. *Enhanced immobilization of arsenic and cadmium in a paddy soil by combined applications of woody peat and Fe(NO_3)$_3$: possible mechanisms and environmental implications*. Sci. Total Environ. 649, 535-543.

WU, C., HUANG, L., XUE, S.G., HUANG, Y.Y., HARTLEY, W., CUIi, M.Q., 2017. *Arsenic sorption by red mud-modified biochar produced from rice straw*. Environ. Sci. Pollut. Res. 24, 18168-18178.

XIAO, M., LI, R.X., YIN, J.L., YANG, J.H., HU, X.Y., XIAO, H.B., WANG, W.L., YANG, T., 2022. *Enhanced photocatalytic oxidation of As(Ⅲ) by TiO_2 modified with Fe_3O_4 through Ti-O-Fe interface bonds*. Colloid. Surface. A., 651, 129678.

XU, Y., LIANG, X., XU, Y., QIN, X., HUANG, Q., WANG, L., SUN, Y., 2017. *Remediation of heavy metal-polluted agricultural soils using clay minerals: a review*. Pedosphere 27, 193-204.

YANG, X. T., XIA, L., LI, J. L., DAI, M., YANG, G. C., SONG, S. X., 2017. *Adsorption of As(III) on porous hematite synthesized from goethite concentrate*. Chemosphere, 169, 188-193.

ZHANG, W.J., JIANG, M.H., 2022. *Efficient remediation of heavily As(III)-contaminated soil using a pre-oxidation and stabilization/solidification technique*. Chemosphere 306, 135598.

ZHAO, F.J., MCGRATH, S.P., MEHARG, A.A., 2010. *Arsenic as a food chain contaminant: mechanism of plant uptake and metabolism and mitigation strategies*. Annu. Rev. Plant Biol. 61, 535-559.

ZHOU, J.J., LIU, Y.W., LI, B.Q., HUANG, W.Y., QIN, J.H., LI, H.S., CHEN, G.K., 2022. *Hydrous zirconium oxide modified biochar for in situ remediation of arsenic contaminated agricultural soil*. J. Environ. Chem. Eng., 10, 108360.